Desantes Fernández, JM.; Serrano Cruz, JR.; Arnau Martínez, FJ.; Piqueras Cabrera, P. (2012). Derivation of the method of characteristics for the fluid dynamic solution of flow advection along porous wall channels. Applied Mathematical Modelling. 36:3134-3152. doi:10.1016/j.apm.2011.09.090.

Derivation of the method of characteristics for the fluid dynamic solution of flow advection along porous wall channels

J. M. Desantes, J. R. Serrano, F. J. Arnau, P. Piqueras*

Universitat Politècnica de València, CMT-Motores Térmicos, Camino de Vera s/n, 46022 Valencia, Spain.

Abstract

This paper describes in detail a novel formulation of the method of characteristics for its application to solve one-dimensional compressible unsteady non-homentropic flow advected along porous wall channels. In particular, the method is implemented into a wall-flow monolith Diesel particulate filter model whose purpose is the pressure drop prediction. The flow inside the monolith channels is considered to be one-dimensional and the flow through the porous wall treated as a source term agree with the Darcy's law. The flow dynamic behaviour at internal nodes of the channels is solved by means of shock capturing methods, whereas the end nodes, or boundary conditions, are solved applying the method of characteristics. The derived solution in this study of the Riemann variables and the entropy level includes the variation along the space-time plane due to cross-section area changes, friction and heat transfer as traditionally stated, but also takes into account the key influence on every line of the flow leaving or entering to the channels through the porous walls.

Keywords: method of characteristics; Diesel particulate filter; wall-flow monolith; pressure drop; porous media

*P. Piqueras. CMT-Motores Térmicos, Universitat Politècnica de València, Camino de Vera s/n, 46022 Valencia, Spain.
Phone: +34 963877650 Fax: +34 963877659 e-mail: pedpicab@mot.upv.es

1. Introduction

The development of the Diesel engine represents one of the most significant improvements of internal combustion engines. Since its invention, it has found its way in numerous applications an benefited from a growing acceptance. Thus, nowadays, it has become the most efficient propulsive system in the automotive sector, both for passenger and heavy duty transport.

To reach its current state of the art, the Diesel engine has undergone an intense evolutionary process, especially in last decades, when environmental issues have leading manufacturers and researchers to the development of new and more efficient technological solutions. New proposals like turbocharging, modern injection systems, electronic control, etc. have contributed to give the public a new positive vision and at the same time have driven towards the emissions reduction.

In the case of Diesel engines, soot particulates are one of the most important emissions. Current and future control emission standards involve a high reduction of this type of emissions to the environment [1]. Only the use of Diesel particulate filters (DPF) ensures the fulfilment of these regulations. The study of the operation principles of this kind of systems was performed at the eighties, but nowadays, and before the need of its use, notable contributions have been carried out inside a multidisciplinary scope. Development aims cover aspects like higher mechanical and chemical durability with high ash accumulation [2], multifunctional monolith reactors [3], advances in porous ceramics materials, catalysts for filtration and regeneration efficiency improvement [4] or analysis of the pre-turbo DPF placement in the exaust line [5]. The analysis of listed phenomena are closely-coupled to the study of the fluid dynamic filter response. The pressure drop induced by the filter results in the engine fuel consumption penalty and hence the understanding of its nature and origin mechanisms becomes fundamental.

As in many other areas of internal combustion engine research, exhaust aftertreatment systems, and inside them DPF, find in numerical calculation tools

a way to choose a few promising solutions to be investigated by concurrent experimental studies. At the same time, they complement the information than experiments can yield. This strategy reverts on costs and time savings.

Inside particulate Diesel after-treatment, wall-flow monolith focuses main research modelling efforts. The reasons are found in the good balance among advantages and drawbacks merged to its use, which has led to its higher widespread commercial implantation [6]. This typology of monolithic filters consists of many small axial parallel channels, typically of square cross-section. Adjacent channels are alternatively plugged at each end in order to force the gas flow through the porous substrate walls. Here the soot particulates are filtrated and accumulated up to its oxidation during the regeneration process.

Depending on the extend of the fluid dynamic study to be performed, the definition and complexity of the DPF models differs. Basic analysis to evaluate the order of magnitude of non-inertial pressure drop at the monolith channels is traditionally raised with simple 0D DPF models, that approximate on an only term the inertial effect at inlet and outlet monolith cross-sections. They focus the analysis on the monolith only and do not cover the whole filter. On the other hand, 1D models allow to deal with inertial effects at inlet and outlet monolith cross-sections independently and the introduction of the inlet and outlet volumes effect. Furthermore, 1D DPF models offer plus information regarding flow velocity or soot distribution profiles, regeneration, temperature gradient analysis, etc, showing high accuracy and reliability. Finally, the use of 3D DPF models is devoted to combine macro-and micro-scale filter geometry involving a detailed porous wall behaviour comprehension.

With respect to 1D DPF models, the Bisset's proposal [7] has become the base of any other later approach because of the rigorous description of flow path and the regeneration process. In this model, the governing equations system is solved under the assumptions of one-dimensional compressible steady non-homentropic flow but neglecting flow velocity effect on stagnation properties. These hypothesis are valid for filter fluid dynamic analysis when it is placed downstream the turbocharger system. Otherwise, the flow is highly pulsating

and unsteadiness and compressibility effects cannot be neglected. Nevertheless the traditional placement of the DPF in the exhaust system is downstream the turbocharger. Therefore, the Bisset's model and other relevant contributions, as the Konstandopoulos' model [8], which provides an analytical solution for clean DPF pressure drop with a one-dimensional incompressible steady isothermal flow approach, have remained as suitable proposals. Other models expect to extend the application conditions of the Bisset's model [9] or directly apply it as an auxiliary tool combined with advanced analysis in filtration and regeneration modelling [10–13]. Additional proposals treat the problem of spacial resolution in the radial monolith direction [14] and acoustic modelling [15].

However, there is a lack of DPF models able to deal with typical flow conditions from internal combustion engines, that are widely accepted to be essentially one-dimensional compressible unsteady and non-homentropic. The DPF device would treat with these flow characteristics in configurations placed upstream the turbocharger [16, 17] or in atmospheric Diesel engines, such as non-road Diesel engines. Only Cunningham [18] and Piscaglia [19] describe models dealing with compressible unsteady flow. However, on the one hand, Cunningham presents a model restricted by the assumption of isothermal flow. On the other hand, Piscaglia approaches a model integrated into a gas dynamics code that solves the fluid dynamics of the DPF with a multi-duct configuration: every single pair of inlet and outlet channels is represented by the combination of several ducts connected to additional transverse ducts representing the porous medium. The interface between the channels and the porous medium ducts is solved by means of boundary conditions for T junctions adapted to the Darcy's law solved applying the method of characteristics (MOC). The main problem of this model is that this representation becomes highly computational effort demanding, a critical problem in 1D gas dynamics codes used for internal combustion engines (ICE) modelling [20, 21]. The reason is the high number of ducts of small length and spatial mesh size and the high number of T junctions of complex characterisation [22].

Under this context, this paper presents a wall-flow DPF model integrated into a gas dynamic code for internal combustion engine modelling. The flow is treated as one-dimensional compressible unsteady and non-homentropic. The model solves the monolith channels as an only duct with loss or gain of flow through the porous wall. This flow is introduced as a source term in the definition of the governing equations whereas the boundary conditions are solved applying the MOC. It is very extended as solver of boundary conditions in gas dynamic models for ICE modelling [19, 22, 23] and applied to transport problems of very different nature, such as flow advection [24], heat radiation [25], convection-diffusion equation solution [26, 27], application in cryogenics [28], non-newtonian viscoelastic fluids [29, 30], turbocharging [31], or shallow flow [32]; its choice responds to the relevant physical information contained into its solution and to the comprehensive and well-documented work existing on the treatment of every kind of boundary regions by means of a MOC-based quasi-steady approach [22, 33].

As main contribution this work presents a detailed derivation of the MOC to solve the end of the channels accounting for the effect of the flow through the porous wall on the Riemann variables and on the entropy level. The proposed formulation of the method may be easily adapted to any other engineering problem of fluid transport in 1D elements with presence of mass flow source terms. Finally, the model in which has been implemented the derived MOC formulation is validated with experimental data coming from a DPF pressure drop characterisation. The aim is to show the sensitivity of the pressure drop prediction in the DPF to the definition of the flow in the boundary conditions vicinity, which underlines the importance of the MOC derivation for porous media.

2. Wall-flow DPF model

In order to introduce the application of the MOC to the solution of the flow advection at porous wall channels, the main features of the fluid dynamic

model of wall-flow monolith, in which it is implemented, is previously presented. The proposed wall-flow DPF model is able to deal with the characteristic high pulsating flow of ICE. The model is integrated into a gas dynamic code named OpenWAM^{TM} [34] (WAM Wave Action Model) which is an open source software developed at author's institution. It solves the one-dimensional compressible unsteady non-homentropic flow governing equations system. Therefore, as any other engine element in gas dynamic models [35], the wall-flow DPF is geometrically represented as a proper combination of 1D elements, solved by means of finite difference numerical methods [20, 22], 0D elements, solved by means of a filling-and emptying model [23], and boundary conditions, solved by means of the MOC [33].

With these basic guide-lines, Figure 1 plots the representation of the wall-flow DPF in OpenWAM^{TM} self-developed interface. In this figure, the small squares represent the boundary conditions and the biggest ones are 0D elements; the 1D elements, ducts or monolith channels, are represented by continuous lines connecting boundary conditions.

This approach includes the modelling of the pressure drop at the inlet and outlet volumes of the DPF. Frequently, they are ducts of large cone angle. Therefore, it prevents from simulating the cones as 1D elements [36, 37]. For that reason, the most simple and suitable solution to integrate such elements into a 0D-1D code consists in simplifying the problem to model the inlet and outlet volumes of the DPF like 0D elements. In every of these volumes two boundary conditions connecting 0D and 1D elements are identified. The definition of discharge coefficients in this kind of boundaries, whose detailed solution can be consulted in [22, 33], allows calculating the pressure drop at the inlet and outlet of every volume. In this way, according to the numbers in Figure 1, it is given that:

- Boundary condition 1 represents the pressure drop due to the expansion of the flow at the inlet cone of the filter.

- Boundary condition 2 represents the pressure drop due to the local contraction of the flow when entering the inlet monolith channels.
- Boundary condition 5 represents the pressure drop due to the local expansion of the flow exiting the outlet monolith channels.
- Boundary condition 6 represents the pressure drop due to the contraction of the flow in the outlet cone of the filter.

Regarding the representation of the monolith, shown in Figure 1, it is assumed, as commonly extended in literature for its simplicity and accuracy, that the flow properties are homogeneous (but time-dependant) at the inlet cross-section of the monolith and there is not heat transfer in the radial direction of the monolith. Under these assumptions all the pairs of inlet-outlet channels have the same thermo-and fluid dynamic behaviour and are represented by the solution of only one of them [7].

Considering Figure 1 nomenclature, the duct 1 has the dimension of an inlet channel, with its outlet end closed (boundary condition 3). The duct 2 represents an outlet channel, with its inlet end closed (boundary condition 4). The flow going into the inlet channels results from dividing the total flow discharged from the inlet volume into the number of inlet channels composing the monolith. The inverse procedure is applied to calculate the flow discharged to the outlet volume from the outlet channels.

The flow through the porous medium is established between the inlet and outlet channels (as grey arrows sketch in Figure 1). The thickness of the porous medium corresponds to the porous wall thickness plus the thickness of the particulate layer, if any.

2.1. Governing equations systems

With these considerations, the governing equations systems given by Eq. (1) to (6) are solved in the inlet and the outlet channels. The conservation equations for one-dimensional compressible unsteady non-homentropic flow are presented in strong conservative form [38].

For the sake of clarity, the spatial mesh structure of the channels is represented in Figure 2. The spatial mesh size is the same both at the inlet and outlet channels and defines the calculation nodes, whose control volumes manage the flow properties going into it and leaving it in the axial and the transverse directions. The flow in the transverse direction is treated as a source term into the one-dimensional conservation equations. The numerical solution of the flow along the monolith channels makes use of two different procedures depending on the node type (internal node or boundary condition). The solution of the governing equations in internal nodes is carried out by means of the two-step Lax&Wendroff method [39], which is a shock-capturing finite difference scheme. The boundary conditions or end nodes of the channels are solved applying the MOC.

- Mass conservation
  - Inlet channel

$$\frac{\partial\left(\rho_i F_i\right)}{\partial t}+\frac{\partial\left(\rho_i u_i F_i\right)}{\partial x}=-4\left(\alpha-2w_p\right)\rho_i u_{w_1} \tag{1}$$

  - Outlet channel

$$\frac{\partial\left(\rho_o F_o\right)}{\partial t}+\frac{\partial\left(\rho_o u_o F_o\right)}{\partial x}=4\alpha\rho_o u_{w_2} \tag{2}$$

  Subscripts i and o are referred to the inlet and outlet channels respectively; ρ is the gas density, u represents the gas velocity and F is the cross-section area of the channel. Regarding the porous medium, whose cross-section geometry for an inlet channel is represented in Figure 3, α is the honeycomb cell size, w_p is the particulate layer thickness and u_w represents the filtration velocity. The subscript 1 is referred to the filtration velocity at the inlet surface of the porous medium whereas the subscript 2 identifies the filtration velocity at the outlet surface, as sketched in Figure 3.

- Momentum conservation

– Inlet channel

$$\frac{\partial\left(\rho_i u_i F_i\right)}{\partial t}+\frac{\partial\left(\rho_i u_i^2 F_i+p_i F_i\right)}{\partial x}-p_i\frac{dF_i}{dx}=-F_w\mu_i u_i \tag{3}$$

– Outlet channel

$$\frac{\partial\left(\rho_o u_o F_o\right)}{\partial t}+\frac{\partial\left(\rho_o u_o^2 F_o+p_o F_o\right)}{\partial x}-p_o\frac{dF_o}{dx}=-F_w\mu_o u_o \tag{4}$$

In Eq. (3) and (4), p represents the gas pressure, μ is the dynamic viscosity and F_w is a momentum transfer coefficient for square cross-section channels whose value is constant (28.454) [7].

- Energy conservation

  – Inlet channel

$$\frac{\partial\left(e_{0i}\rho_i F_i\right)}{\partial t}+\frac{\partial\left(h_{0i}\rho_i u_i F_i\right)}{\partial x}=q_i\rho_i F_i-4\left(\alpha-2w_p\right)h_{0w}\rho_i u_{w_1} \tag{5}$$

  – Outlet channel

$$\frac{\partial\left(e_{0o}\rho_o F_o\right)}{\partial t}+\frac{\partial\left(h_{0o}\rho_o u_o F_o\right)}{\partial x}=q_o\rho_o F_o+4\alpha h_{0w}\rho_o u_{w_2} \tag{6}$$

The specific stagnation internal energy of the gas is e_0 whereas h_0 represents the specific stagnation enthalpy; q is the heat per unit of time and area transferred between the gas and the porous wall.

2.2. Numerical solution at internal channel nodes

The solution of every conservation equations system at internal nodes of the channels is carried out applying the two-step Lax&Wendroff method [39, 40]. However, both the inlet and outlet channels are related by the flow through the porous medium. It results in the coupling of the corresponding governing equations systems defining an only control volume for the solver, as Figure 2 shows.

The physical coupling between channels is performed by means of the modelling of the pressure drop taking place along the porous medium. Inside it the

flow is considered to have a quasi-steady behaviour [19, 40]. The solution of the governing equations of the inlet and outlet channels at time t provides the values of p_i and p_o at every calculation node. Therefore, the pressure drop taking place at every control volume represented for every pair of inlet and outlet nodes is known, as suggested in Figure 2, and allows calculating the filtration velocity applying the Darcy's law and the continuity equation on the porous medium [41].

Under these considerations, the two-step Lax&Wendroff method is formulated at every channel node as:

$$\mathbf{W}_{j+\frac{1}{2}}^{n+\frac{1}{2}} = \frac{\mathbf{W}_j^n + \mathbf{W}_{j+1}^n}{2} - \frac{\Delta t}{2\Delta x}\left(\mathbf{F}_{j+1}^n - \mathbf{F}_j^n\right) - \frac{\Delta t}{4}\left(\mathbf{C}_j^n + \mathbf{C}_{j+1}^n\right) - \\ - \frac{\Delta t}{4}\left(\mathbf{C}_{w_k,j}^n + \mathbf{C}_{w_k,j+1}^n\right) \tag{7}$$

$$\mathbf{W}_j^{n+1} = \mathbf{W}_j^n - \frac{\Delta t}{\Delta x}\left(\mathbf{F}_{j+\frac{1}{2}}^{n+\frac{1}{2}} - \mathbf{F}_{j-\frac{1}{2}}^{n+\frac{1}{2}}\right) - \frac{\Delta t}{2}\left(\mathbf{C}_{j-\frac{1}{2}}^{n+\frac{1}{2}} + \mathbf{C}_{j+\frac{1}{2}}^{n+\frac{1}{2}}\right) - \\ - \frac{\Delta t}{2}\left(\mathbf{C}_{\mathbf{w_k},j-\frac{1}{2}}^n + \mathbf{C}_{\mathbf{w_k},j+\frac{1}{2}}^n\right) \tag{8}$$

In Eq. (7) and (8), $\mathbf{W}$ and $\mathbf{F}$ are the field variable and the flux vectors respectively. The source term vectors are represented by the vector $\mathbf{C}$, which includes friction, heat transfer and area change terms, and the vector $\mathbf{C_{w_k}}$, which contains the source terms corresponding to the mass and energy flow through the porous medium. The subscript k takes the value 1 for the inlet wall surface and 2 for the outlet wall surface; subscripts n and j define the calculation mesh identifying the time level and the axial position respectively.

The space-time mesh for the formulation of the two-step Lax&Wendroff is represented in Figure 4 for a pair of inlet-outlet channels. It corresponds to the traditional computational stencil for the calculation of the gas properties at every internal node of a 1D element with the addition of the porous medium

influence. According to the definition of the method, at every channel, either inlet or outlet, the solution at node j and time step $n+1$ is obtained in two steps. In the first step the solution at time step $n+\frac{1}{2}$ is obtained at virtual nodes $j-\frac{1}{2}$ and $j+\frac{1}{2}$ from the flow properties calculated at the previous time step (n) at nodes $j-1$, j and $j+1$. In the second-step, the flow properties at node j at time step $n+1$ are determined from the virtual solutions at coordinates $(j-\frac{1}{2}, n+\frac{1}{2})$ and $(j+\frac{1}{2}, n+\frac{1}{2})$.

The porous medium flow terms are governed by the value of the filtration velocity on every wall surface, which at node j and time step n depends on the gas pressure of the inlet and outlet channels (Darcy's law) at the same node and time step and on the continuity equation applied to the porous medium [41]. If there is a shift in the axial direction between the inlet and the outlet channel nodes because of the plug length, then an interpolation procedure would be applied in order to obtain the flow properties of the adjacent channel for the same axial location in which the porous medium is solved. This situation is shown in the spatial mesh depicted in channels of Figure 5.

Due to the quasi-steady behaviour of the flow inside the porous wall and according to Eq. (8), the second step of the Lax-Wendroff method is solved at the control volume of the node j considering that the filtration velocity variation during the interval time between n and $n+1/2$ is negligible. This assumption contributes to reduce the computational effort and has not effect on the solution due to the quasi-steady porous medium behaviour. With regard to the calculation of the filtration velocities, grey dashed arrows in Figure 4 point out that their value at time level n is calculated on every surface of the porous wall from the gas pressure at the inlet and outlet channels at time level n in the same axial position.

3. Derivation of the method of characteristics with mass flow through porous walls

The solution of the wave motion inside the channels has been described on the basis of the application of a finite difference numerical method in order to obtain an accurate and reliable solution. To ensure the appropriate propagation of this solution along the modelled configuration (i.e. the exhaust line) also the boundaries need to watch over their definition.

As represented in Figure 1, there are four boundary conditions in every pair of inlet-outlet channels. From the numeration of this figure:

- Boundary conditions 2 and 5 model the junction between the cones (0D elements) and the channels (1D elements). The porous walls of the control volume of these boundary conditions are in contact with the plugged axial section of the adjacent channels. Therefore, the information towards the boundary from the channels is only partially affected by the presence of flow through the porous medium.

- Boundary conditions 3 and 4 model the closed ends of the channels due to the plug. These boundary conditions are fully affected by the presence of flow through the porous medium.

As commonly extended in gas dynamic codes, the solution of the boundary conditions is carried out applying the MOC [22, 23]. This method has to be specifically formulated in order to account for the presence of flow through the channel walls, since its porous nature affects the variation of the Riemann variables and the entropy level along the time-space plane.

As first step, the departure point of the characteristic lines and the pathline has to be calculated at time t at every channel end (the calculated lines at every channel end depends on the flow sense). From these points, the Riemann variables (λ and β) and the entropy level (A_A) reach the end channels (boundary condition) at time $t + \Delta t$. It allows the specific solution for the boundary

condition (0D-1D junction or closed end). This procedure is sketched in Figure 5 and can be consulted in detail in [42].

The second stage involves the calculation of the Riemann variables and the entropy level values at their departure point at time t. Following equations show this calculation, where A and U represent the dimensionless speed of sound and the dimensionless gas velocity respectively.

- Incident characteristic

$$\lambda_i = A_i + \frac{\gamma+1}{2}U_i \qquad \lambda_o = A_o + \frac{\gamma+1}{2}U_o \tag{9}$$

- Reflected characteristic

$$\beta_i = A_i - \frac{\gamma+1}{2}U_i \qquad \beta_o = A_o - \frac{\gamma+1}{2}U_o \tag{10}$$

- Entropy level

$$A_{A_i} = A_i \left(\frac{p_{ref}}{p_i}\right)^{\frac{\gamma-1}{2\gamma}} \qquad A_{A_o} = A_o \left(\frac{p_{ref}}{p_o}\right)^{\frac{\gamma-1}{2\gamma}} \tag{11}$$

In a standard 1D element, with no mass flow source terms, if friction and heat transfer are not considered, the entropy level remains constant in the time-space plane and the flow is said to be homentropic. Furthermore, in ducts of constant cross-section, the value of the Riemann variables would be also invariant through the characteristic lines. Under these assumptions, the value of the Riemann variables and the entropy level at their corresponding end at time $t + \Delta t$ would be the same as at their departure point at time t.

In the general case of non-homentropic flow, both the characteristics lines and the pathline change their slope along the time-step and the distance up to the duct end. These variations can be evaluated as function of the heat transfer and the friction transfer processes. The characteristics lines are additionally modified by the cross-section area change and the entropy level variation.

In the case of a 1D element with mass flow source terms along its length (for the specific case of this work with mass flow through porous walls), the flow is

always non-homentropic due to the effect of the mass flow variation on the fluid properties. This effect has to be taken into account in the quantification of the Riemann variables and the entropy level values at the ends at time $t + \Delta t$, as Eq. (12), (13) and (14) point out:

$$\lambda_{end} = \lambda_{dp} + d\lambda_{friction} + d\lambda_{heat\ transfer} + d\lambda_{cross-section} + \\ + d\lambda_{A_A} + d\lambda_{porous\ medium} \tag{12}$$

$$\beta_{end} = \beta_{dp} + d\beta_{friction} + d\beta_{heat\ transfer} + d\beta_{cross-section} + \\ + d\beta_{A_A} + d\beta_{porous\ medium} \tag{13}$$

$$A_{A_{end}} = A_{A_{dp}} + dA_{A_{friction}} + dA_{A_{heat\ transfer}} + dA_{A_{porous\ medium}} \tag{14}$$

3.1. Governing equations in non-conservative law form for porous wall channels

The expression to quantify the value of the porous medium effect needs of the derivation of the MOC. This method is based on the non-conservative law form of the conservation equations for one-dimensional compressible unsteady flow derived for a perfect gas. Under the assumption of gradual cross-section area variation, the mass conservation equation for porous wall square channels can be written as:

- Mass conservation

$$\frac{\partial \rho}{\partial t} + u\frac{\partial \rho}{\partial x} + \rho\frac{\partial u}{\partial x} + \frac{\rho u}{F}\frac{dF}{dx} = (-1)^i \frac{4\rho u_{w_{2-i}}}{\alpha - 2w_p i} \tag{15}$$

The subscript i takes the value 1 for an inlet channel or 0 for an outlet channel. The momentum conservation equation in non-conservative law form is obtained from its conservative law form expanding and combining with the non-conservation law form of the mass conservation equation (15). Finally, taking into account the friction process, yields

- Momentum conservation

$$\frac{\partial u}{\partial t} + u\frac{\partial u}{\partial x} + \frac{1}{\rho}\frac{\partial p}{\partial x} = -\frac{F_w \nu u}{F} - (-1)^i \frac{4u_{w_{2-i}} u}{\alpha - 2w_p i} \tag{16}$$

where ν represents the kinematic viscosity of the fluid.

In the same way, the non-conservative law form of the energy equation is derived from the conservative law form combining with the mass and momentum equations. Initially, the conservative law form of the energy conservation, including heat transfer between the gas and the channel walls, can be written as:

- Energy conservation

$$\frac{\partial \left[F\rho\left(c_v T + \frac{u^2}{2}\right)\right]}{\partial t} + Fu\frac{\partial \left[\rho\left(c_v T + \frac{u^2}{2} + \frac{p}{\rho}\right)\right]}{\partial x} +$$

$$+\rho\left[c_v T + \frac{u^2}{2} + \frac{p}{\rho}\right]\frac{d\left(Fu\right)}{dx} = q\rho F + (-1)^i 4\left(\alpha - 2w_p i\right)\rho u_{w_{2-i}} h_{0w} \tag{17}$$

The cross-section area of the channels is assumed to be constant in time for the solution of the boundaries. This hypothesis is completely fulfilled in output channels. It becomes acceptable in the case of the inlet channels because of the difference in the order of magnitude between the integral time-step for the governing equations and the characteristic time of the accumulation-regeneration processes. Therefore, dividing Eq. (17) by ρ and F gives

$$\left(c_v T + \frac{u^2}{2}\right)\left[\frac{1}{\rho}\left(\frac{\partial \rho}{\partial t} + u\frac{\partial \rho}{\partial x}\right) + \frac{1}{F}\frac{d\left(Fu\right)}{dx}\right] + \frac{D}{Dt}\left(c_v T + \frac{u^2}{2}\right) =$$

$$= q + (-1)^i \frac{4u_{w_{2-i}} h_{0w}}{\alpha - 2w_p i} - \frac{u}{\rho}\frac{\partial p}{\partial x} - \frac{p}{\rho F}\frac{d\left(Fu\right)}{dx} \tag{18}$$

The term between square brackets in Eq. (18) coincides with the derivative terms in the mass conservation equation (15) divided by ρ. Thus, Eq. (18) becomes

$$\left(c_v T + \frac{u^2}{2}\right)\left((-1)^i \frac{4u_{w_{2-i}}}{\alpha - 2w_p i}\right) + \frac{D}{Dt}\left(c_v T + \frac{u^2}{2}\right) =$$

$$= q + (-1)^i \frac{4u_{w_{2-i}} h_{0w}}{\alpha - 2w_p i} - \frac{u}{\rho}\frac{\partial p}{\partial x} - \frac{p}{\rho F}\frac{d(Fu)}{dx} \tag{19}$$

The total derivative of the specific stagnation internal energy in Eq. (19) can be expanded as

$$\frac{D}{Dt}\left(c_v T + \frac{u^2}{2}\right) = \frac{D}{Dt}(c_v T) + \frac{D}{Dt}\left(\frac{u^2}{2}\right) = \frac{D}{Dt}(c_v T) + u\frac{Du}{Dt} \tag{20}$$

where the total derivative of the flow velocity in the channel is obtained of the non-conservation law form of the momentum conservation equation (16) and expressed as:

$$\frac{Du}{Dt} = -\frac{1}{\rho}\frac{\partial p}{\partial x} - \frac{F_w \nu u}{F} - (-1)^i \frac{4u_{w_{2-i}} u}{\alpha - 2w_p i} \tag{21}$$

Eq. (19) combined with Eq. (20) and (21) and rearranging can be written as:

$$\frac{D}{Dt}(c_v T) + \frac{p}{\rho F}\frac{d(Fu)}{dx} =$$

$$= q - (-1)^i \frac{4u_{w_{2-i}}(e_0 - h_{0w})}{\alpha - 2w_p} + u\left(\frac{F_w \nu u}{F} + (-1)^i \frac{4u_{w_{2-i}} u}{\alpha - 2w_p i}\right) \tag{22}$$

The difference between the specific stagnation internal energy of the flow inside the inlet channel and the specific stagnation enthalpy of the flow going into the porous wall depends on the kinetic energy and the pressure. In the output channel, this difference depends also on the difference between the temperature of the flow inside the channel and the temperature of the flow incorporated from the porous channel wall. Nevertheless the difference in temperature is only relevant at regeneration conditions. Therefore, taking into account that this work does not deal with regeneration conditions, for the sake of keeping

homogeneity between the inlet and the outlet channels formulation, Eq. (22) can be stated as

$$\frac{D}{Dt}\left(c_v T\right) + \frac{p}{\rho F}\frac{d\left(Fu\right)}{dx} =$$

$$= q - \left(-1\right)^i \frac{4u_{w_{2-i}}}{\alpha - 2w_p i}\left(\frac{u^2 - u_{w_{2-i}}^2}{2} - \frac{p}{\rho}\right) + u\left(\frac{F_w \nu u}{F} + \left(-1\right)^i \frac{4u_{w_{2-i}} u}{\alpha - 2w_p i}\right) \quad (23)$$

Next, Eq. (23) is multiplied by $(\gamma - 1)\rho$. The resulting derivative term can be written as

$$\left(\gamma - 1\right)\rho\left[\frac{D}{Dt}\left(c_v T\right) + \frac{p}{\rho F}\frac{d\left(Fu\right)}{dx}\right] = \rho\frac{D}{Dt}\left[\left(\gamma - 1\right)\left(c_v T\right)\right] + \left(\gamma - 1\right)\frac{p}{F}\frac{d\left(Fu\right)}{dx} =$$

$$= \rho\frac{D}{Dt}\left(\frac{p}{\rho}\right) + \left(\gamma - 1\right)\frac{p}{F}\frac{d\left(Fu\right)}{dx} = \frac{Dp}{Dt} - \frac{p}{\rho}\frac{D\rho}{Dt} + \left(\gamma - 1\right)\frac{p}{F}\frac{d\left(Fu\right)}{dx} =$$

$$= \frac{Dp}{Dt} - \frac{p}{\rho}\frac{D\rho}{Dt} + \left(\gamma - 1\right)p\left(\frac{u}{F}\frac{\partial F}{\partial x} + \frac{\partial u}{\partial x}\right) \quad (24)$$

The spatial derivatives relative to the cross-section area and the flow velocity can be expressed as function of the mass conservation equation in non-conservative law form:

$$\frac{Dp}{Dt} - \frac{p}{\rho}\frac{D\rho}{Dt} + \left(\gamma - 1\right)p\left(\frac{u}{F}\frac{\partial F}{\partial x} + \frac{\partial u}{\partial x}\right) =$$

$$= \frac{Dp}{Dt} - \frac{p}{\rho}\frac{D\rho}{Dt} + \left(\gamma - 1\right)p\left(\left(-1\right)^i \frac{4u_{w_{2-i}}}{\alpha - 2w_p i} - \frac{1}{\rho}\frac{D\rho}{Dt}\right) =$$

$$= \frac{Dp}{Dt} - \frac{\gamma p}{\rho}\frac{D\rho}{Dt} + \left(-1\right)^i \frac{4u_{w_{2-i}}}{\alpha - 2w_p i}\left(\gamma - 1\right)p \quad (25)$$

Taking into account the result in Eq. (25), introducing the definition of the speed of sound, the energy conservation equation for porous wall square channels is finally formulated in non-conservation law form as:

$$\frac{Dp}{Dt} - a^2\frac{D\rho}{Dt} = (\gamma - 1)\,\rho\left(q - (-1)^i\,\frac{4u_{w_{2-i}}}{\alpha - 2w_p i}\left(\frac{u^2 - u_{w_{2-i}}^2}{2}\right) + \right.$$

$$\left. + u\left(\frac{F_w \nu u}{F} + (-1)^i\,\frac{4u_{w_{2-i}} u}{\alpha - 2w_p i}\right)\right) \tag{26}$$

3.2. Characteristic lines and pathline time-space variation in porous wall channels

Eq. (15), (16) and (26) constitute a quasi-linear equations system in partial derivatives of hyperbolic type. Performing the appropriate transformations, which can be consulted in [22, 33], the first-order differential equations system composed by Eq. (27), (28) and (29) is obtained:

- Equation along a time-space plane line with slope $u + a$

$$\frac{Dp}{Dt} + \rho a\frac{Du}{Dt} + \rho a\frac{F_w \nu u}{F} - (-1)^i\,\frac{4\rho u_{w_{2-i}} a^2}{\alpha - 2w_p i} + \frac{\rho a^2 u}{F}\frac{dF}{dx} +$$

$$+ (-1)^i\,\rho a\frac{4u_{w_{2-i}} u}{\alpha - 2w_p i} - (\gamma - 1)\,\rho\left(q - (-1)^i\,\frac{4u_{w_1}}{\alpha - 2w_p i}\left(\frac{u^2 - u_{w_{2-i}}^2}{2}\right) + \right.$$

$$\left. + u^2\left(\frac{F_w \nu}{F} + (-1)^i\,\frac{4u_{w_{2-i}}}{\alpha - 2w_p i}\right)\right) = 0 \tag{27}$$

- Equation along a time-space plane line with slope $u - a$

$$\frac{Dp}{Dt} - \rho a\frac{Du}{Dt} - \rho a\frac{F_w \nu u}{F} - (-1)^i\,\frac{4\rho u_{w_{2-i}} a^2}{\alpha - 2w_p i} + \frac{\rho a^2 u}{F}\frac{dF}{dx} -$$

$$- (-1)^i\,\rho a\frac{4u_{w_{2-i}} u}{\alpha - 2w_p i} - (\gamma - 1)\,\rho\left(q - (-1)^i\,\frac{4u_{w_1}}{\alpha - 2w_p i}\left(\frac{u^2 - u_{w_{2-i}}^2}{2}\right) + \right.$$

$$\left. + u^2\left(\frac{F_w \nu}{F} + (-1)^i\,\frac{4u_{w_{2-i}}}{\alpha - 2w_p i}\right)\right) = 0 \tag{28}$$

- Equation along a time-space plane line with slope u

$$\frac{Dp}{Dt} - a^2 \frac{D\rho}{Dt} - (\gamma - 1)\,\rho \left(q - (-1)^i \frac{4u_{w_{2-i}}}{\alpha - 2w_p i} \left(\frac{u^2 - u_{w_{2-i}}^2}{2} \right) + \right.$$

$$\left. + u^2 \left(\frac{F_w \nu}{F} + (-1)^i \frac{4u_{w_{2-i}}}{\alpha - 2w_p i} \right) \right) = 0 \tag{29}$$

This system is usually applied in dimensionless form, but including previously the concept of entropy level. It is defined as the speed of sound that could be reached if the flow would suffer an adiabatic and reversible expansion up to an arbitrary reference pressure.

Taking into account the entropy level and performing the transformations described in [22, 33], the previous equations system is reduced to the following definitions:

- Incident characteristic, λ:

$$da + \frac{\gamma - 1}{2} du = a \frac{da_A}{a_A} + \frac{\gamma - 1}{2} \left[-\frac{au}{F} \frac{dF}{dx} + (-1)^i \frac{4u_{w_{2-i}} a}{\alpha - 2w_p i} + \right.$$

$$+ \left((\gamma - 1)\,\frac{u}{a} - 1 \right) \frac{F_w \nu u}{F} - (-1)^i \left(1 - (\gamma - 1)\,\frac{u}{a} \right) \frac{4u_w u}{\alpha - 2w_p i} +$$

$$\left. + \frac{\gamma - 1}{a} \left(q - (-1)^i \frac{4u_{w_{2-i}}}{\alpha - 2w_p i} \left(\frac{u^2 - u_{w_{2-i}}^2}{2} \right) \right) \right] dt \tag{30}$$

- Reflected characteristic, β:

$$da - \frac{\gamma - 1}{2} du = a \frac{da_A}{a_A} + \frac{\gamma - 1}{2} \left[-\frac{au}{F} \frac{dF}{dx} + (-1)^i \frac{4u_{w_{2-i}} a}{\alpha - 2w_p i} + \right.$$

$$+ \left((\gamma - 1)\,\frac{u}{a} + 1 \right) \frac{F_w \nu u}{F} + (-1)^i \left((\gamma - 1)\,\frac{u}{a} + 1 \right) \frac{4u_{w_{2-i}} u}{\alpha - 2w_p i} +$$

$$\left. + \frac{\gamma - 1}{a} \left(q - (-1)^i \frac{4u_{w_{2-i}}}{\alpha - 2w_p i} \left(\frac{u^2 - u_{w_{2-i}}^2}{2} \right) \right) \right] dt \tag{31}$$

- Entropy level, A_A:

$$da_A = \frac{\gamma-1}{2}\frac{a_A}{a^2}\left(q-(-1)^i\frac{4u_{w_{2-i}}}{\alpha-2w_p i}\left(\frac{u^2-u_{w_{2-i}}^2}{2}\right)+\right.$$

$$\left.+u^2\left(\frac{F_w\nu}{F}+(-1)^i\frac{4u_{w_{2-i}}}{\alpha-2w_p i}\right)\right)dt \tag{32}$$

Next, a series of dimensionless variables are defined from the reference speed of sound (a_{ref}) and the reference length (x_{ref}), which is given by the spatial mesh size applied to the channel:

1. Dimensionless speed of sound: $A = \frac{a}{a_{ref}}$
2. Dimensionless velocity: $U = \frac{u}{a_{ref}}$
3. Dimensionless entropy level: $A_A = \frac{a_A}{a_{ref}}$
4. Dimensionless axial dimension: $X = \frac{x}{x_{ref}}$
5. Dimensionless time-step: $dZ = a_{ref}\frac{dt}{x_{ref}}$

From these quantities, Eq. (30), (31) and (32) can be rewritten, after some arrangement, in the form:

- Incident characteristic, λ:

$$dA+\frac{\gamma-1}{2}dU = A\frac{dA_A}{dA}-\frac{\gamma-1}{2}\frac{AU}{F}\frac{dF}{dX}dZ+$$

$$+\frac{\gamma-1}{2}\left[(-1)^i\frac{4u_{w_{2-i}}A}{\alpha-2w_p i}+\left((\gamma-1)\frac{U}{A}-1\right)\frac{F_w\nu U}{F}+\right.$$

$$-(-1)^i\left(1-(\gamma-1)\frac{U}{A}\right)\frac{4u_{w_{2-i}}U}{\alpha-2w_p i}+$$

$$\left.+\frac{(\gamma-1)}{A}\left(\frac{q}{a_{ref}^2}-(-1)^i\frac{4u_{w_{2-i}}}{\alpha-2w_p i}\left(\frac{U^2-\frac{u_{w_{2-i}}^2}{a_{ref}^2}}{2}\right)\right)\right]\frac{x_{ref}}{a_{ref}}dZ \tag{33}$$

- Reflected characteristic, β:

$$dA - \frac{\gamma-1}{2}dU = A\frac{dA_A}{dA} - \frac{\gamma-1}{2}\frac{AU}{F}\frac{dF}{dX}dZ +$$

$$+\frac{\gamma-1}{2}\left[(-1)^i \frac{4u_{w_{2-i}}A}{\alpha - 2w_p i} + \left((\gamma-1)\frac{U}{A}+1\right)\frac{F_w \nu U}{F} +\right.$$

$$+(-1)^i\left((\gamma-1)\frac{U}{A}+1\right)\frac{4u_{w_{2-i}}U}{\alpha-2w_p i}+$$

$$\left.+\frac{(\gamma-1)}{A}\left(\frac{q}{a_{ref}^2} - (-1)^i\frac{4u_{w_{2-i}}}{\alpha-2w_p i}\left(\frac{U^2 - \frac{u_{w_{2-i}}^2}{a_{ref}^2}}{2}\right)\right)\right]\frac{x_{ref}}{a_{ref}}dZ \qquad (34)$$

- Entropy level, A_A:

$$dA_A = \frac{\gamma-1}{2}\frac{A_A}{A^2}\left[\frac{q}{a_{ref}^2} - (-1)^i\frac{4u_{w_{2-i}}}{\alpha-2w_p i}\left(\frac{U^2 - \frac{u_{w_{2-i}}^2}{a_{ref}^2}}{2}\right) +\right.$$

$$\left.+U^2\left(\frac{F_w\nu}{F} + (-1)^i\frac{4u_{w_{2-i}}}{\alpha-2w_p i}\right)\right]\frac{x_{ref}}{a_{ref}}dZ \qquad (35)$$

The value of the Riemann variables and the entropy level at the end of the channels at time $t+\Delta t$ from the departure point at time t is obtained integrating Eq. (33), (34) and (35). This proposed formulation includes properly the effect of the flow through the porous medium.

As general approach, the model deals with this solution to the problem taking into account that the terms derived from the flow through the porous medium will affect during the whole time-step (Δt). However, two cases have to be considered for the boundary conditions connecting the inlet and outlet volumes of the DPF to the monolith channels. Firstly, the porous medium terms will become null if the spatial mesh size is equal or shorter than the plug length. The reason is that, under this condition, the filtration velocity is zero in the region affected by the boundary. This case is represented in Figure 6(a),

which represents the calculation of the reflected characteristic in the inlet node of an inlet channel when the spatial mesh size is less than the plug length.

Secondly and on the contrary, if the spatial mesh size at this sort of ends is longer than the plug length, the mass flow through the porous medium will probably have influence on the value of the Riemann variables and the entropy level, but only during the interval time given by

$$\Delta t' = \frac{x_{dp} - x_{plug}}{u_{prop}} \tag{36}$$

where u_{prop} is the propagation speed at the departure point of the characteristic or path line being calculated. This situation is represented in Figure 6(b) for the calculation of the reflected characteristic in the inlet node of an inlet channel. According to it, x_{dp} is the distance from the departure point to the calculated end and x_{plug} is the plug length.

4. Experimental validation and discussion

The importance of the MOC derivation to consider the porous medium behaviour is highlighted on the basis of the pressure drop characterisation of an standard DPF in a steady cold flow test rig. The main characteristics of the DPF are listed in Table 1.

The comparison between experimental data and modelling results is shown in Figure 7(a). This plot relates the Reynolds number (Re) of the flow in the inlet duct to the filter with the pressure drop taking place at the system. High accuracy has been found between the predicted pressure drop by the DPF model and the experimental measurements. The difference with respect to experimental data is limited to 50 Pa in absolute value inside the tested Re range, which is similar to that found during engine operation.

The pressure drop calculation with the presented DPF model has been carried out defining the different contributions to the pressure drop. Known the value of the wall permeability and the correlation to model the pressure drop

due to fluid friction with porous walls in square section channels, it has only remained the definition of the inertial contributions by means of the corresponding discharge coefficients. From the mathematical point of view, there are a high number of possible combinations of their values to obtain the desired flow condition (Re). In order to prevent from the possible dispersion in the solution and a lack of physical meaning, the setup has been carried out on the basis of a set of phenomenological criteria. These criteria are referred to the expected qualitative distribution of the different contributions to the pressure drop in a clean wall-flow DPF [43]. Results shown in Figure 7(b) agree with these criteria. It is observed that the non-inertial pressure drop, which includes the friction and the Darcy's law contributions, varies between 85% and 50% from low to high Re. On the other hand, the inertial pressure drop at the monolith outlet is double than the inertial pressure drop at the monolith inlet at high Re, growing this ratio as the Re diminishes.

With the purpose to discern how the MOC formulation influences on the characterisation of the pressure drop in a DPF, Figure 8 shows again the predicted pressure drop and its decomposition but for the case of frictionless and adiabatic processes in the solution of the MOC boundary conditions. With respect to the heat transfer, no much differences were expected since in the characterisation of the DPF pressure drop the tests are conducted to be at ambient temperature conditions. Therefore, the temperature gradient between the gas and the porous wall tends to be null. As regards the friction, the performed calculation, which covers a wide Re range, allows concluding that its influence both on the pressure drop prediction and distribution is small on the boundary condition solution.

4.1. Effect of flow through the porous wall on MOC solution

Figure 9 shows the results that the model would provide with the previously obtained setup for discharge coefficients but with the traditional MOC formulation. It means that the effect of the flow through the porous walls has been not taken into account in the solution of the boundary conditions.

Results in Figure 9(a) evidences that this kind of solution gives rise to the over-prediction of the pressure drop, which increases further with the Re. Plot b) establishes that, for the same Re, the pressure drop increase is mainly located at the channels, whose contribution (non-inertial) to the pressure drop grows clearly in percentage. The increase of these term is around a 5% in absolute percentage value, independently of the Re.

The reason explaining the behaviour shown by the model when the MOC is not adapted to the porous medium has been explored analysing the flow velocity field at the inlet and outlet channels and the filtration velocity field on the porous wall. The results are represented in Figure 10, which provides a comparison between the results of MOC formulation for porous channels and the traditional MOC. Regarding the filtration velocity, only the filtration velocity on the inlet wall surface is shown versus the dimensionless channel length. The filtration velocity on the outlet wall surface is ommited for simplicity sake. It has also to be noted that between the inlet and the outlet channels there is a displacement that corresponds to the plug length. Therefore the axial position x in the inlet channel should be compared with the axial position $x - x_{plug}$ of the outlet channel.

The analysed operating points are identified by the pressure drop imposed to the global system (inlet duct, DPF and outlet duct), which is the same independently of the MOC formulation. Despite it and as detailed in Table 2, the pressure drop at the channels (non-inertial) is higher when the traditional MOC is applied. It results in a slightly lower Re at the inlet duct to the DPF for the same pressure drop and, therefore, means a lower mass flow rate through the system. According to this response, the obtained flow velocity fields in channels are always of lower magnitude when the traditional MOC is applied.

On the other hand, the prediction of the filtration velocity is very similar at internal channel nodes at high Re but becomes into an underestimation at low Re. The characteristics of this profile indicate that both the friction pressure drop and the pressure drop induced by the porous medium are lessened in these nodes with respect to that provided by the porous wall MOC. However, the

filtration velocity is higher in the axial locations of the closed ends, mainly in the case of the inlet channel end since it contributes to stop the flow.

The increase of the filtration velocity at channel ends, to which the traditional MOC leads, results in the increase of the non-inertial pressure drop through the porous medium. This was the conclusion pointed out by Figure 9 in conditions of same Re comparing traditional and porous wall MOC. Figure 11 states this previous conclusion also in the case of the same pressure drop in the whole system. It shows the pressure field in the inlet and outlet channels for the analysed operating points. As expected from velocity profiles, the pressure drop at the boundary control volume is artificially increased due to the overestimation of the pressure at inlet channels ends and the underestimation at outlet ones with respect to the solution provided by the proposed porous medium MOC.

Furthermore, due to the fact that the mass flow has decreased for the same pressure drop at the system, it is followed that also the inertial pressure drop contribution has decreased. Therefore, the higher pressure drop through the porous medium, which is caused by the boundaries solution and summarised in Table 2, explains the stabilisation of the system in an operating point of lower mass flow.

On the other hand, Figure 11(a) and in lesser degree plot b) show also a relevant characteristic of the pressure field for the given porous wall structure, which is defined by the wall permeability. At these plots, which depict the pressure fields in operating conditions at high Re, the pressure increases inside the inlet channel and as a consequence the filtration velocity increases also monotonically. As the Re number grows, the flow mass accumulation capacity at the volume defined by the inlet channels takes importance, dominating over the pressure drop caused by the friction process. On the contrary, as the Re diminishes, the friction process together with the loss of flow through the porous wall become dominant and control the pressure drop and therefore the filtration velocity profile. The behaviour at these operating conditions results in the decrease of the static pressure along the inlet channel, as plots c) and d) present. The response shown by the DPF at high mass flow operating points justifies the

convenience of properly treat the flow as compressible in order to deal with the fluid dynamic description. The accuracy of this description is essential to ensure the reliability of further studies dealing with soot filtration deposition and ash distribution along the porous wall, particulate layer properties, pressure drop dynamics under loading or regeneration conditions, hot spots generation, etc.

Finally, a sensitivity study carried out on the value of the wall permeability allow extending the conclusions regarding the influence of the MOC formulation to a range of wall permeability covering the state of the art order of in wall-flow DPFs.

Figure 12 represents the flow velocity and pressure field in the inlet and outlet channels and the filtration velocity field for two different pressure drops imposed to the system when the wall permeability is equal to 2.49e-14 m^2, i.e one order of magnitude lower than the wall permeability of the reference DPF. The differences between the porous medium MOC and the traditional MOC can be observed, being evident the artificial distortion of the filtration velocity at the end of the channel.

Regarding the influence of the wall permeability, its reduction leads to an increase of the pressure drop across the porous wall. On the one hand, it means lower flow velocity in comparison with the same pressure drop imposed to the system shown in Figure 10 (Δp=6500 Pa and Δp=3850 Pa). On the other hand, the pressure drop field is quasi-constant along the channel. As a consequence, the filtration velocity is also quasi-constant along the wall and the flow velocity field variation tends to be linear both in the inlet and the outlet channels.

Figure 13 shows the results for the same cases of pressure drop imposed on the system but being the wall permeability one order of magnitude higher than in the case of the reference DPF (k_w = 2.49e-12 m^2). The non-physical solution provided by the traditional MOC can be identified again on the filtration velocity at the end of the channel.

As a consequence of the wall permeability increase, the pressure drop across the porous medium is very reduced being higher the flow velocity and the air mass flow in comparison with the reference DPF. The increase of the wall per-

meability has also led to an important variation of the flow field along the channels.

Up to the 80% of the channel length, the pressure drop across the porous medium is quasi-constant with length. It gives rises to a quasi-linear variation of the flow velocity field in the inlet and the outlet channels along this length. In this section of the channel length, the filtration velocity is very low because of the pressure drop distribution and the flow is accumulated at the end of the inlet channel. As a result, an increase of pressure takes place in this region. The subsequent increase of pressure drop at the end of the channels produces the corresponding increase of filtration velocity and flow mass across the porous medium. It causes a sudden decrease of the flow velocity in the inlet channel and the corresponding increase in the outlet channel.

5. Summary and conclusions

The paper presents a model solving one-dimensional compressible unsteady non-homentropic flow for wall-flow monolith Diesel particulate filters. The description is focused on the derivation of the MOC, which is applied in the solution of the boundary conditions. The main contribution has been to adapt the MOC to the porous nature of the monolith walls in order to obtain a reliable accurate characterisation of the DPF flow dynamics. The porous medium retains the soot particulate from the exhaust gases due to the flow crossing it from the inlet to the outlet channels leading to a non-neglecting pressure drop.

The inclusion of the flow through the porous medium as an additional term into the formulation of the MOC affects both the Riemann variables and the entropy level variation in the time-space plane. The importance of this calculation has been underlined with an experimental validation based on the measuring of the pressure drop of a standard DPF, which is performed under cold steady flow conditions. The use of a 1D model has allowed identifying and quantifying the different contributions to the pressure drop. At first step, the presented work has evidenced that friction phenomena, traditionally considered in the MOC, is

not a process with high influence on the solution of the boundary conditions of the monolith channels. When it is neglected, the pressure drop characterisation is sparsely affected.

On the contrary, it has been stated that when the traditional MOC is used, without considering the porous medium, the model highly over-predicts the pressure drop due to an artificial increase of the non-inertial contribution. In particular, it has been found that internal nodes are not sensitively affected. Nevertheless, the calculation nodes at boundary conditions introduce a spurious distortion of the pressure field in the channels that leads to the increase of the Darcy's law contribution because of the corresponding wrong evaluation of the filtration velocity.

References

[1] Regulation (EC) N 715/2007 of the European Parliament and of the Council of 20 June 2007 on type approval of motor vehicles with respect to emissions from light passenger and commercial vehicles (Euro 5 and Euro 6) and on access to vehicle repair and maintenance information. Official Journal of the European Union, June 2007.

[2] A.G. Konstandopoulos, M. Kostoglou, N. Vlachos, E. Kladopoulou, Advances in the science and technology of Diesel particulate filter simulation, Advances in Chemical Engineering, 33 (2007) 284-294.

[3] K. Nakatani, S. Hirota, S. Takeshima, K. Itoh, T. Tanaka, K. Dohmae, Simultaneous PM and NOx reduction system for Diesel engines, SAE Technical Paper 2002-01-0957, 2002.

[4] S. Lorentzou, C. Pagkoura, A.G. Konstandopoulos, J. Boettcher, Advanced catalyst coatings for Diesel particulate filters, SAE Technical Paper 2008-01-0843, 2008.

[5] V. Bermúdez, J.R. Serrano, P. Piqueras, O. García-Afonso, Assessment by means of gas dynamic modelling of a pre-turbo Diesel particulate filter configuration in a turbocharged HSDI Diesel engine under full-load transient operation, Proceedings of the Institution of Mechanical Engineers, Part D: Journal of Automobile Engineering, June 27, 2011, doi: 10.1177/0954407011402278.

[6] M. Murtagh, Diesel particulate filters (DPF): A short course, Diesel particulate and NOx emissions course, University of Leeds, Ann Arbor, MI, 2002.

[7] E.J. Bisset, Mathematical model of the thermal regeneration of a wall-flow monolith Diesel particulate filter, Chemical Engineering Science 39 (1984) 1233-1244.

[8] A.G. Konstandopoulos, J.H. Johnson, Wall-flow Diesel particulate filters - Their pressure drop and collection efficiency, SAE Technical Paper 890405, 1989.

[9] G. Gaiser, P. Mucha, Prediction of pressure drop in Diesel particulate filters considering ash deposit and partial regeneration, SAE Technical Paper 2004-01-0158, 2004.

[10] G.C. Koltsakis, A.M. Stamatelos, Modes of catalytic regeneration in Diesel particulate filters, Industrial and Engineering Chemistry Research 36 (1997) 4155-5165.

[11] A.G. Konstandopoulos, M. Kostuglou, Reciprocating flow regeneration of soot filters, Combustion and Flame 121 (2000) 488-200.

[12] Z. Guo, Z. Zhang, A one-dimensional numerical model for Diesel particulate trap performance study during loading and regeneration, International Journal of Engine Research 6 (2005) 247-262.

[13] M. Zheng, S. Banerjee, Diesel oxidation catalyst and particulate filter modeling in active –Flow configurations, Applied Thermal Engineering, 20 (2009) 3021-3025.

[14] A.G. Konstandopoulos, E. Skaperdas, M. Masoudi, Inertial contributions to the pressure drop of Diesel particulate filters, SAE Technical Paper 2001-01-0909, 2001.

[15] S. Allam, M. Åbom. Acoustic modelling and testing of Diesel particulate filters, Journal of Sound and Vibration 288 (2005) 255-273.

[16] F. Payri, J.M. Desantes, J. Galindo, J.R. Serrano, Exhaust manifold of a turbo-supercharged reciprocating engine, Patent application WO 2010/092201. Priority date 13/02/2009. Oficina Española de Patentes y Marcas, 2009.

[17] M.N. Subramaniam, V. Joergl, P. Keller, O. Weber, T. Toyoshima, C.D. Vogt, Feasibility assessment of a pre-turbo after-treatment system with a 1D modeling approach, SAE Technical Paper 2009-01-1276, 2009.

[18] P. Cunningham, P. Meckl, 1-D dynamic Diesel particulate filter model for unsteady pulsating flow, SAE Technical Paper 2007-01-1140, 2007.

[19] F. Piscaglia, G. Ferrari, A novel 1D approach for the simulation of unsteady reacting flows in Diesel exhaust after-treatment systems, Energy 34 (2009) 2051-2062.

[20] J.R. Serrano, F.J. Arnau, P. Piqueras, A. Onorati, G. Montenegro, 1D gas dynamic modelling of mass conservation in engine duct systems with thermal contact discontinuities, Mathematical and Computer Modelling 49 (2009) 1078-1088.

[21] J. Galindo, J.R. Serrano, F.J. Arnau, P. Piqueras, High-frequency response of a calculation methodology for gas dynamics based on Independent Time Discretisation, Mathematical and Computer Modelling 50 (2009) 812-822.

[22] D.E. Winterbone, R.J. Pearson, Theory of engine manifold design: wave action methods for IC engines, Professional Engineering Publishing, 2000.

[23] J. Galindo, J.R. Serrano, F.J. Arnau, P. Piqueras, Description and analysis of a one-dimensional gas-dynamic model with Independent Time Discretization, Proceedings of the ASME Internal Combustion Engine Division 2008 Spring Technical Conference ICES2008, 2008.

[24] M.R. Kaazempur-Mofrad, C.R. Ethier, An efficient characteristic Galerkin scheme for the advection equation in 3-D, Computer Methods in Applied Mechanics and Engineering, 191(46) (2002) 5345-5363.

[25] K.M. Katika, L. Pilon, Modified method of characteristics in transient radiation transfer, Journal of Quantitative Spectroscopy and Radiative Transfer 98 (2006) 220-237.

[26] L. Banas, Solution of convection–diffusion equation by the method of characteristics, Journal of Computational and Applied Mathematics 168 (2004) 31-39.

[27] H. Rui, A conservative characteristic finite volume element method for solution of the advection–diffusion equation, Computer Methods in Applied Mechanics and Engineering, 197(45-48) (2008) 3862-3869.

[28] M.Y. Xu, Y.L. He, Z.Q. Chen, Analysis of an orifice pulse tube refrigerator using the method of characteristics, Cryogenics 39 (1999) 751-757.

[29] F.G. Basombrío, Flows of viscoelastic fluids treated by the method of characteristics, Journal of Non-Newtonian Fluid Mechanics 39 (1991) 17-54.

[30] A. Machmoum, D. Esselaoui, Finite element approximation of viscoelastic fluid flow using characteristics method, Computer Methods in Applied Mechanics and Engineering, 190(42) (2001) 5603-5618.

[31] T. Katranik, Improved model to determine turbine and compressor boundary conditions with the method of characteristics, International Journal of Mechanical Sciences 48 (2006) 504-516.

[32] A. Mohammadian, D.Y. Le Roux, M. Tajrishi, A conservative extension of the method of characteristics for 1-D shallow flows, Applied Mathematical Modelling, 31(2) (2007) 332-348.

[33] R.S. Benson, The thermodynamics and gas dynamics of internal-combustion engines, vol. 1. Clarendon Press, Oxford, 1982.

[34] OpenWAM website, CMT-Motores Térmicos (Universitat Politècnica de València), www.openwam.org (2011).

[35] J. Galindo, J.R. Serrano, F.J. Arnau, P. Piqueras, Description of a Semi-Independent Time Discretization methodology for a one-dimensional gas dynamics model, Journal of Engineering for Gas Turbines and Power 131 (2009) 034504.

[36] F. Payri, J. Galindo, J.R. Serrano, F.J. Arnau, Analysis of numerical methods to solve one-dimensional fluid-dynamic governing equations under impulsive flow in tapered ducts, International Journal of Mechanical Science 46 (2004) 981-1004.

[37] A.J. Torregrosa, J.R. Serrano, F.J. Arnau, J.V. Romero, Experimental validation of a new semi-implicit CE-SE scheme for the calculation of unsteady one-dimensional flow in tapered-ducts, International Journal for Numerical Methods in Engineering 74 (2008) 1473-1494.

[38] Ll. Gascón, J.M. Corberán, Construction of second-order TVD schemes for nonhomogeneous hyperbolic conservation laws, Journal of Computational Physics 172 (2001) 261-297.

[39] P.D. Lax, B. Wendroff, Systems of conservation laws, Communications on Pure and Applied Mathematics 17 (1964) 381-398.

[40] J.V. Romero, M.D. Roselló, F.J. Arnau, P. Piqueras, Study of finite difference numerical method solution applied to one-dimensional compressible flow in ducts with mass flow source terms, Modelling 2009, Roznov Pod Radhostem, Czech Republic, 2009.

[41] A.J. Torregrosa, J.R. Serrano, F.J. Arnau, P. Piqueras, A fluid dynamic model for unsteady compressible flow in wall-flow Diesel particulate filters, Energy 36 (2011) 671-684.

[42] A. Broatch, J.R. Serrano, F.J. Arnau, D. Moya, Time-domain computation of muffler frequency response: comparison of different numerical schemes, Journal of Sound and Vibration 305 (2007) 333-347.

[43] M. Masoudi, Hydrodynamics of Diesel particulate filters, SAE Technical Paper 2002-01-1016, 2002.

0D	zero-dimensional
1D	one-dimensional
3D	three-dimensional
a	speed of sound
a_A	entropy level
a_{ref}	reference speed of sound
A	dimensionless speed of sound
A_A	dimensionless entropy level
c_v	specific heat at constant volume
$\mathbf{C}$	source term vector
$\mathbf{C_{w_k}}$	porous wall source term vector
DPF	Diesel particulate filter
e_0	specific stagnation internal energy
F	cross-section area
$\mathbf{F}$	flux vector
F_w	momentum transfer coefficient for square channels
h_0	specific stagnation enthalpy
ICE	internal combustion engine
$l^*_{channel}$	dimensionless channel length
MOC	method of characteristics
p	gas pressure
q	heat per unit of time and area
Re	Reynolds number
t	time dimension
T	gas temperature
u	gas velocity
u_{prop}	propagation wave speed
u_w	filtration velocity

U	dimensionless flow velocity
x	axial dimension
x_{dp}	distance from the departure point to the calculated end
x_{plug}	plug length
x_{ref}	reference axial dimension
X	dimensionless axial dimension
w_p	particulate layer thickness
w_w	porous wall thickness
$\mathbf{W}$	field variable vector
WAM	Wave Action Model
z	transverse coordinate
Z	dimensionless time

Greek letters

α	honeycomb cell size
β	reflected characteristic (Riemann variable)
Δp	pressure drop
Δt	time-step
$\Delta t'$	interval time of influence of porous medium on boundary solution
γ	specific heat ratio
λ	incident characteristic (Riemann variable)
μ	dynamic viscosity
ν	kinematic viscosity
ρ	gas density

Subscripts

dp	characteristic line or pathline departure point
i	inlet channel
j	index for calculation node

k index for porous medium wall surface

n index for time level

o outlet channel

p particulate layer

w porous wall

List of Tables

List of Figures

Table 1: Geometrical characteristics of the experimentally characterised DPF.

Length	m	0.2
Diameter	m	0.132
Volume	l	2.74
Cross-section	m^2	0.0137
Plug length	mm	3.2
Wall permeability	m^2	2.49e-13
Cell density	$cpsi$	200
Filter cell size	mm	1.486
Wall thickness	mm	0.31
Number of channels	–	4246
Filtration area	m^2	2.5
Inlet cone volume	cm^3	500
Outlet cone volume	cm^3	450

Table 2: Definition of the operating points whose velocity profiles are represented in Figure 10.

	Porous wall MOC		Traditional MOC	
Δp_{system}	$Re_{inlet\ DPF}$	$\Delta p_{non-inertial}$	$Re_{inlet\ DPF}$	$\Delta p_{non-inertial}$
$[Pa]$	$[-]$	$[Pa]$	$[-]$	$[Pa]$
6500	150300	1434	148047	1696
3850	112725	1049	110546	1232
1550	65750	603	63190	684
490	30060	278	28464	329

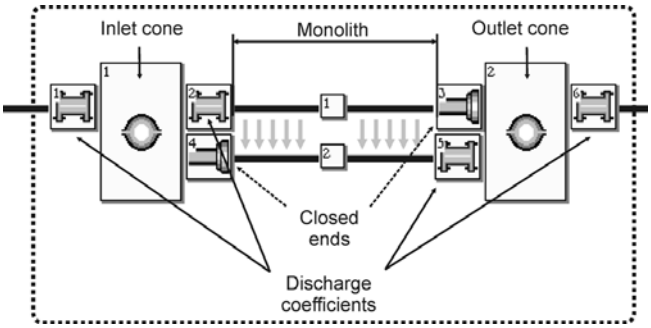

Figure 1: DPF model scheme into the gas dynamics code OpenWAM^{TM} as combination of 1D, 0D and boundary conditions elements.

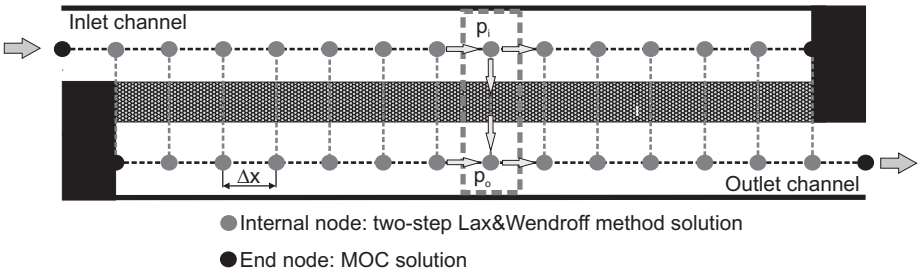

Figure 2: Spatial mesh for the discrete solution of the governing equations in a single pair of inlet-outlet channels of the wall-flow monolith.

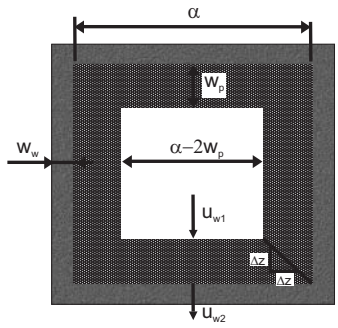

Figure 3: Cross-section geometry of an inlet channel and filtration velocity through the porous medium.

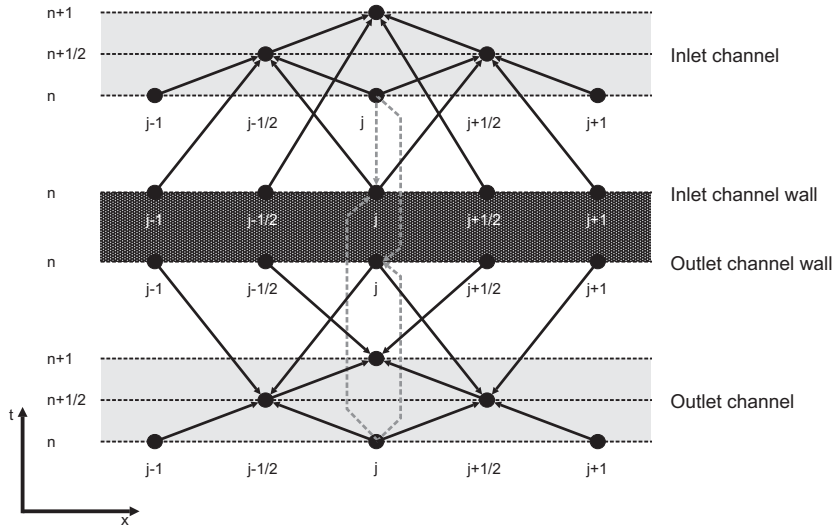

Figure 4: Computational stencil of the two-step Lax&Wendroff method to obtain the flow properties in the internal nodes of the inlet and outlet channels of wall-flow monoliths.

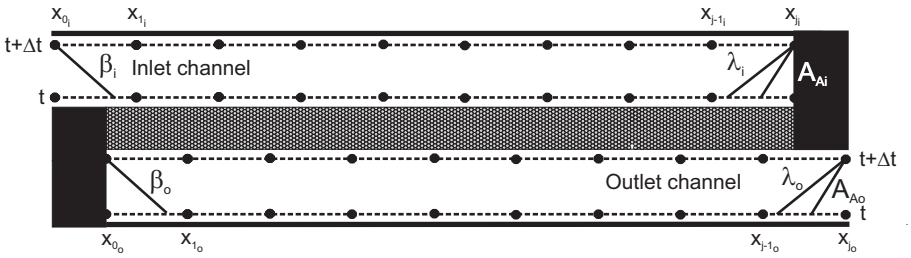

Figure 5: Representation of the departure point of the characteristic lines (λ and β) and the pathline (A_A) at the ends of a pair of inlet-outlet channels of the monolith. Standard flow conditions are assumed with a sense from left to right.

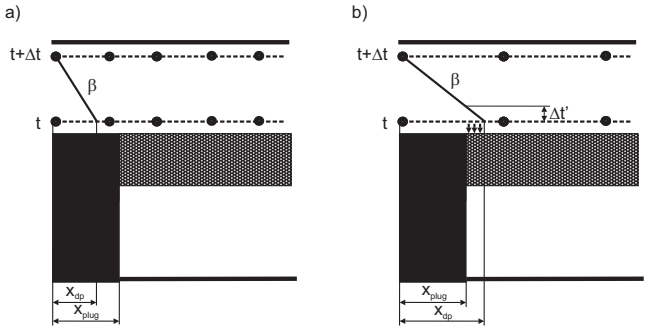

Figure 6: Schematic representation of the reflected characteristic calculation at the boundary of the inlet channel connecting with the inlet DPF cone: a) $x_{dp} \leq x_{plug}$: no influence of porous medium terms; b) $x_{dp} > x_{plug}$: interval time of calculation affected by the mass flow through the porous medium.

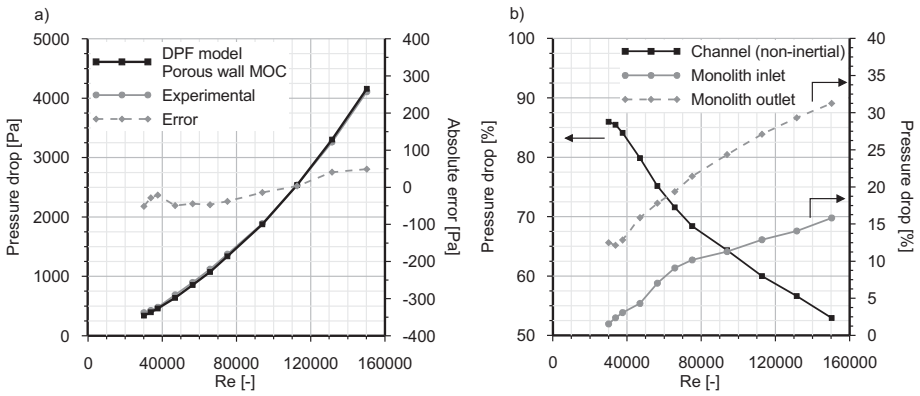

Figure 7: Comparison between experimental and modelled filter pressure drop under cold steady flow conditions: proposed MOC formulation for porous walls. a) Pressure drop prediction and absolute error. b) Distribution of the monolith pressure drop contributions vs. Re of the flow in the inlet duct to the DPF.

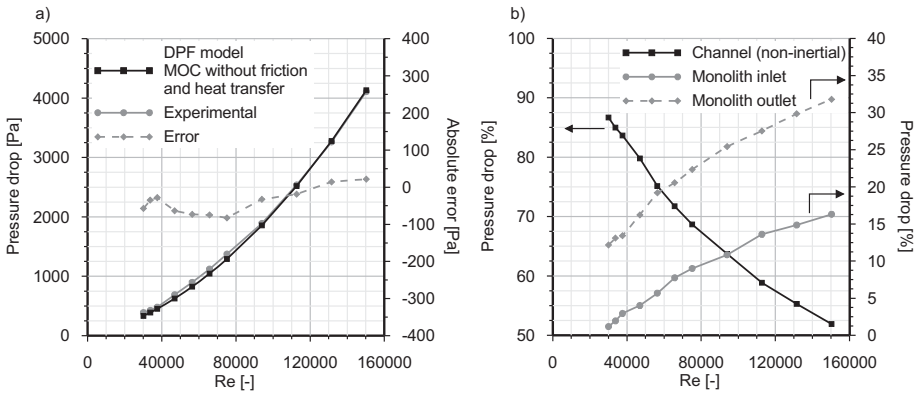

Figure 8: Comparison between experimental and modelled filter pressure drop under cold steady flow conditions: proposed MOC formulation for porous walls but for frictionless and adiabatic processes. a) Pressure drop prediction and absolute error. b) Distribution of the monolith pressure drop contributions vs. Re of the flow in the inlet duct to the DPF.

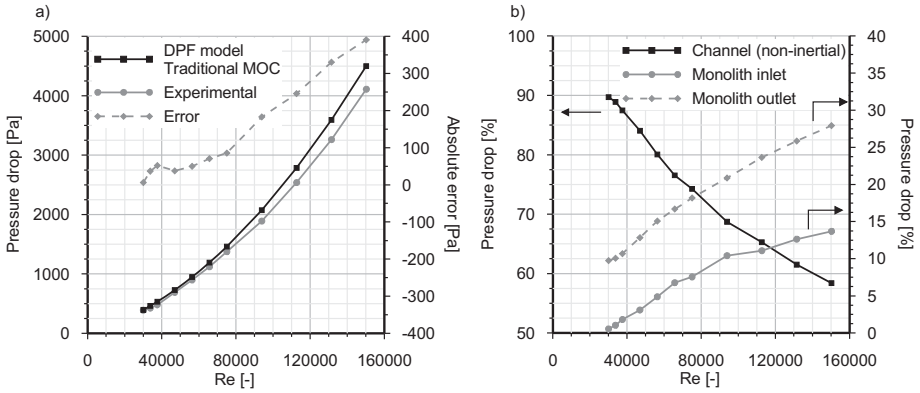

Figure 9: Comparison between experimental and modelled filter pressure drop under cold steady flow conditions: traditional MOC formulation. a) Pressure drop prediction and absolute error. b) Distribution of the monolith pressure drop contributions vs. Re of the flow in the inlet duct to the DPF.

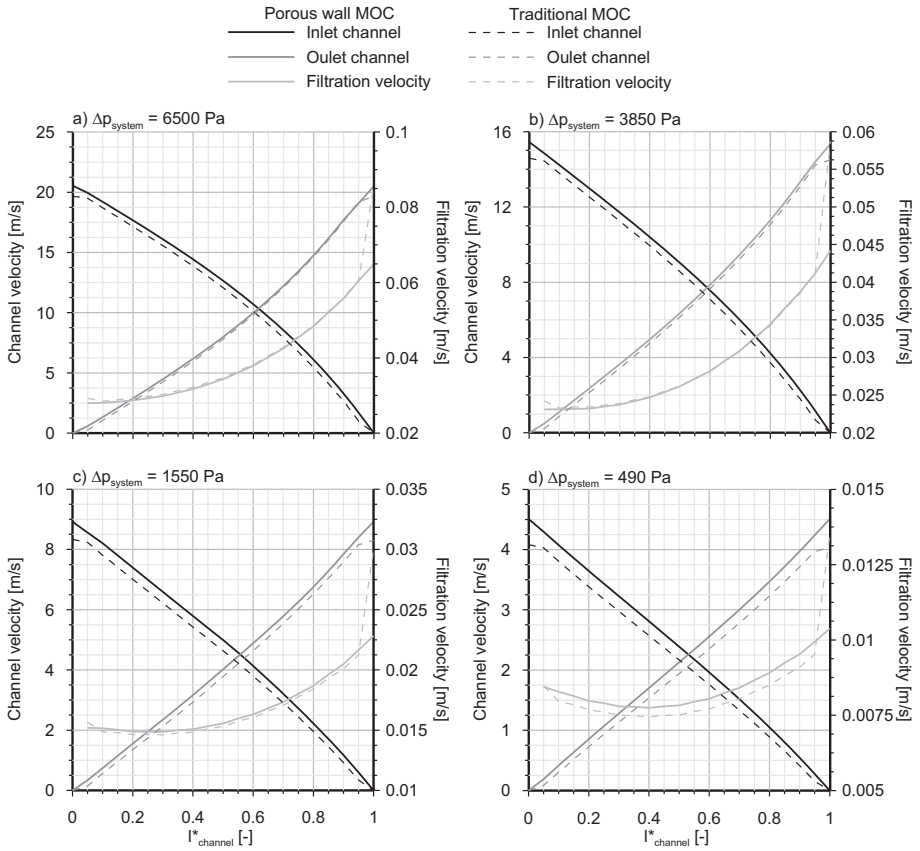

Figure 10: Flow velocity field at inlet and outlet channels and filtration velocity field as function of the MOC formulation imposing several Δp to the system.

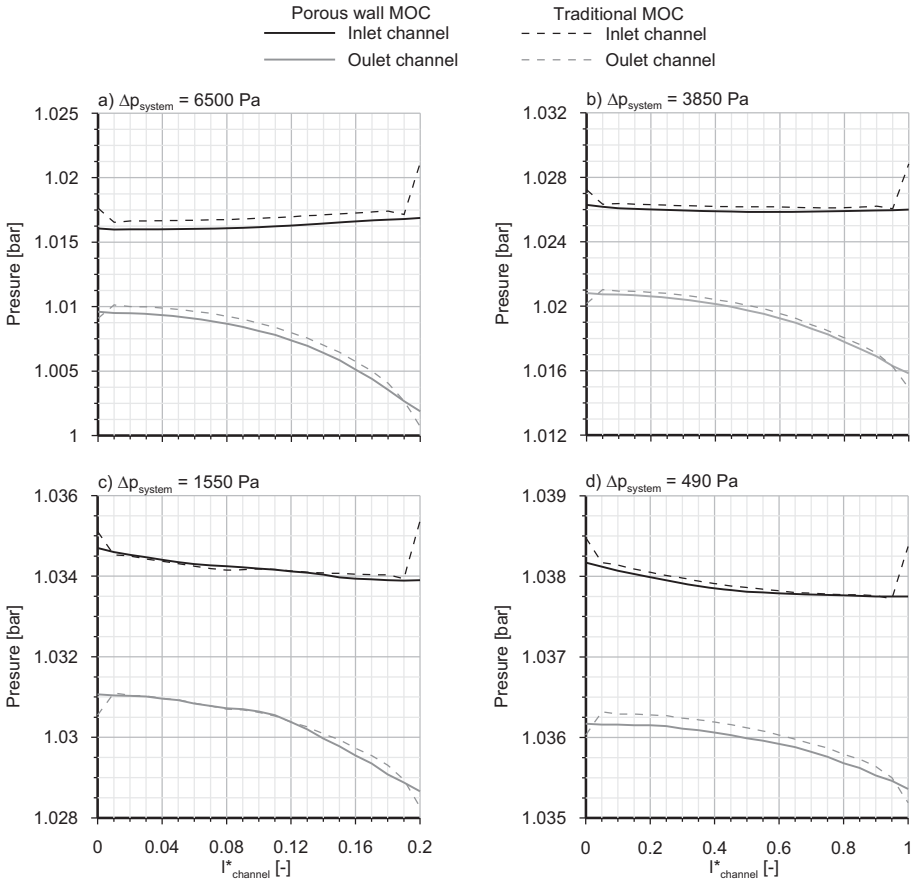

Figure 11: Pressure field at inlet and outlet channels as function of the MOC formulation imposing several Δp to the system.

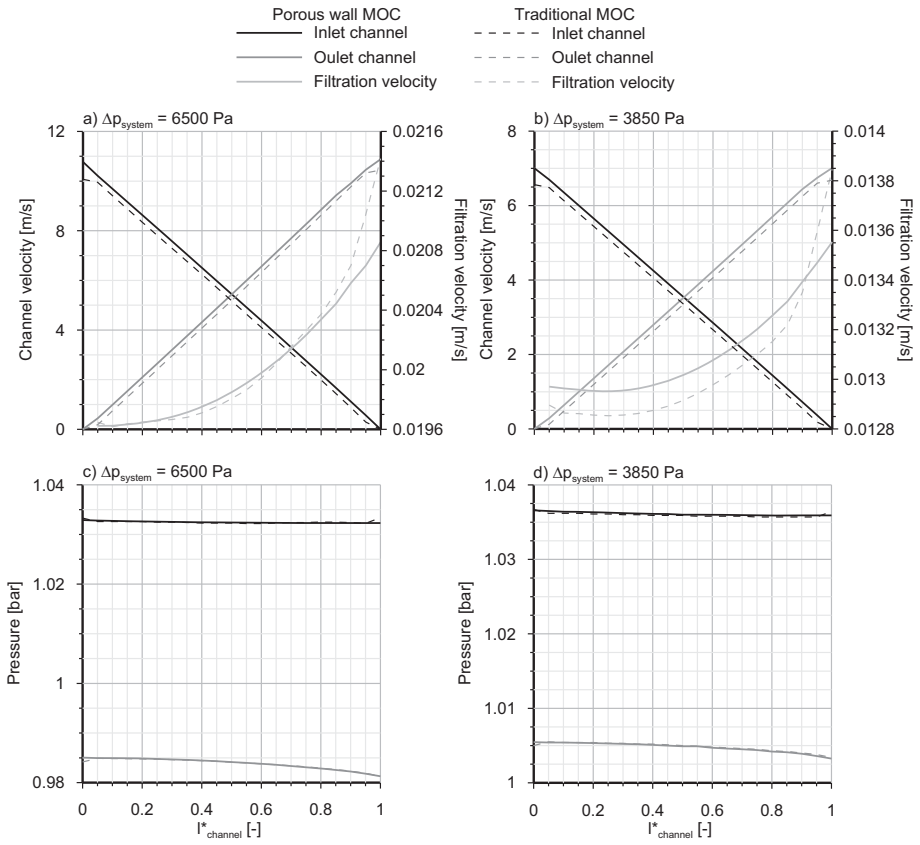

Figure 12: Flow velocity and pressure field at inlet and outlet channels and filtration velocity field as function of the MOC formulation imposing several Δp to the system being the wall permeability k_w = 2.49e-14 m^2.

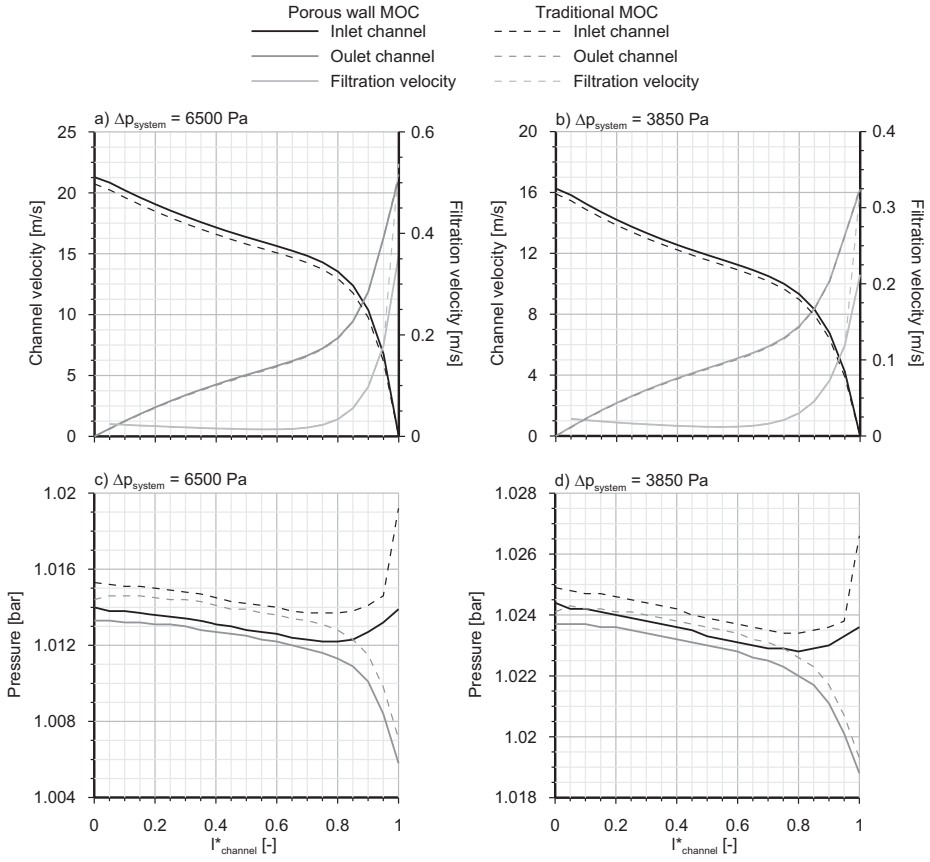

Figure 13: Flow velocity and pressure field at inlet and outlet channels and filtration velocity field as function of the MOC formulation imposing several Δp to the system being the wall permeability k_w = 2.49e-12 m^2.